Theses and Dissertations

12-2011

Degradation of Polystyrene Foam under Radiant Heat Flux

James Butler
University of Arkansas, Fayetteville

Follow this and additional works at: http://scholarworks.uark.edu/etd

 Part of the Complex Fluids Commons, and the Structural Materials Commons

Degradation of Polystyrene Foam under Radiant Heat Flux

Degradation of Polystyrene Foam under Radiant Heat Flux

A thesis submitted in partial fulfillment
of the requirements for the degree of
Masters of Science in Chemical Engineering

By

James B. Butler
University of Arkansas
Bachelor of Science in Chemical Engineering, 2003

December 2011
University of Arkansas

Abstract

As the demand for liquefied natural gas has increased, safety concerns about the performance of transport vessels under fire conditions have been raised. Current codes for the sizing of the pressure relief systems require that the vessels are able to withstand an emmissive heat flux of $108\,\mathrm{kW/m^2}$ and do not take into account the effects of insulation loss due to thermal decomposition of the insulation materials. To address this possible oversight in the current code models were presented to a working group organized by the Society of International Gas Tanker and Terminal Operators Ltd. focusing on the decomposition rate of the polystyrene insulation used on many of these shipping vessels under fire conditions. The working group considered a range of heat flux from liquified natural gas pool fires with fluxes up to $300\,\mathrm{kW/m^2}$. However, without experimental verification of the behavior of the polystyrene insulation under these conditions the working group deferred the concerns stating that, "a better understanding of the foam plastic insulation vulnerability to heating is required to adequately assess the hazards that could result from loss of insulation effectiveness with fire exposure".

Using an experimental procedure adapted from the work of Braumen, Chen and Matzinger on the thermal response of solid polystyrene under fire conditions, a rod driven apparatus was constructed to measure the regression rates of both solid and foamed samples of polystyrene as a function of external heat flux. From a plot of this data the heat loss to the surroundings and the heat of vaporization of the samples were calculated. Comparisons of the heats of vaporization were made to the values reported here as well as to independent differential scanning calorimetry and thermogravimetric analysis data.

It was shown that the mass loss rate of the foamed polystyrene is essentially the same as the solid polystyrene when exposed to high rates of heating. The only significant difference between the two forms of polystyrene is in the linear regression rate which is higher in the foamed polystyrene by approximately the same ratio as the densities, about 40 to 1. The heat of vaporiza-

tion for the solid polystyrene and the foamed polystyrene were found to be $1592\,\mathrm{J/g}$ and $1693\,\mathrm{J/g}$ respectively. The comparison to the differential scanning calorimetry data for the samples was within 10%. The linear regression of the foamed polystyrene was found to be $0.138\,\mathrm{cm/min}$ for each $\mathrm{kW/m^2}$ of absorbed heat.

This thesis is approved for recommendation
to the Graduate Council

Thesis Director:

_____

Dr. Jerry Havens, Ph.D.

Thesis Committee:

_____

Dr. Heather Walker, Ph.D.

_____

Dr. Greg Thoma, Ph.D.

_____

Dr. Robert Beitle, Ph.D.

_____

Dr. Rick Couvillion , Ph.D.

Thesis Duplication Release

     I hereby authorize the University of Arkansas Libraries to duplicate this thesis when needed for research and/or scholarship.

Agreed   _____
          James B. Butler

Acknowledgements

    I would like to thank Dr. Jerry Havens for his support in completing this Master's thesis. His guidance in determining the key factors involved in this process were invaluable. I would also like to thank Dr. Heather Walker for educating me in proper record keeping. Without her insight on keeping detailed records many of the nuances of this experiment would likely have been lost.

Contents

List of Figures

List of Tables

Terms and Definitions

Abbreviations

BCM : Braumen, Chen, and Matzinger 1983

DNV: Det Norske Veritas

DSC: Differential Scanning Calorimetry

EPS: Expanded Polystyrene

IGC Code: International Code for the Construction and Equipment of Ships Carrying Liquefied
Gases in Bulk

IMO: International Maritime Organization

LFC: Lost Foam Casting

LNG: Liquid Natural Gas

PRV: Pressure Relief Valve

PS: Polystyrene

SIGTTO: Society of International Gas Terminal and Tanker Operators

TGA : Thermo-gravimetric Analysis

XPS : Extruded Polystyrene

Symbols

A_q : Cross Section Area of Quartz Sleeve, cm^2

A_s : Cross Section Area of Sample, cm^2

ε : emissivity

H_{vap} : heat of vaporization, J/g

H_{rvum} : heat required to vaporize a unit mass, J/g

j : emissive power, kW/m^2

$\dot{m}$: mass flux, g/(cm^2 s)

m_p : Slope of Pump Calibration Curve, 0.01401 cm/s

m_r : Slope of Radiometer Calibration Curve, 22.13 kW/(m^2 mV)

$\dot{q}_{ext}$: incident heat flux, W/cm^2

$\dot{q}_l$: absorbed heat flux, W/cm^2

R_{avg} : Average Pump Reading

ρ : Density of Sample, g/cm^3

R_i : Pump Reading at a Given Time

σ : Stephan-Boltzmann constant, 5.67×10^{-8} J/(s m^2 K^4)

T : surface temperature, W/cm^2

t_f : Time of Final Measurement, s

t_i : Time of Measurement, s

t_{i+1} : Time of Next Measurement, s

v_r : Ram Velocity, cm/s

V_r : Radiometer Voltage Reading, mV

Chapter 1

Introduction

A growing demand in the liquefied natural gas (LNG) import/export market has caused a resurgence in concerns about the safety surrounding LNG trade [10]. To these concerns more rigorous methods have been applied to understanding the hazards that surround the existing and future infrastructure supporting the safe economic transport of LNG. In 2004 concerns about the performance of polymeric foams, used as insulation in LNG shipping vessels, under fire conditions were expressed. The increased boil off due to a partial or complete loss of the insulation is not taken into account in the current regulations for the sizing of pressure relief valves (IMO IGC Code 8.5). A debate over the possibility and effects of fire on the LNG vessels followed but as no direct data on the failure rate of the polymeric insulation was available these concerns were deferred stating, "a much better understanding of the temporal response of foam plastic insulation materials is necessary" [12]. This thesis attempts to provide that understanding by reporting on the response rate of polystyrene foam to an applied radiant heat flux.

1.1 Liquefied Natural Gas

Liquefied natural gas (LNG) is a cryogenic, condensed form of natural gas that has been cooled to approximately $-161\,^\circ$C. It is made up primarily of methane with small amounts of ethane, propane, butane, nitrogen and sometimes trace amounts of other light end hydrocarbons. In its liquid form it has a density that is approximately 45% that of water and as a result pools on top of water when spilled. Natural gas is colorless, odorless, non-toxic, and non-carcinogenic. It's main component, methane, is lighter than air and has a positive buoyancy under normal atmospheric conditions. Methane has flammable limits between 4 and 16 percent in air. [13] It is over all considered one of the cleaner forms of fossil fuel.

The commercial practice of liquefying natural gas first began as a peak shaving practice by

energy companies. The earliest LNG plant was built in West Virginia in 1914 but the first of these plants designed for full scale commercial operation was built in Cleveland, OH in 1941. [7] As the process of liquefaction of natural gas raised the density of the fuel approximately 600 times, it opened up new opportunities for the economic shipping of LNG over large distances that were too costly to satisfy with traditional natural gas pipelines. To this end, in January of 1959, the Methane Pioneer made its inaugural voyage transporting $5000\,m^3$ of LNG from Lake Charles, LA to Canvey Island, UK [11]. This successful long distance transport of LNG via ship set the stage for the maritime commercial shipping of LNG. Currently there are over 300 LNG carriers in service. These are primarily composed of two major types of cargo containment systems: moss spheres and membrane systems. The moss sphere design makes up almost half of the current fleet at this point and is the focus of the current debate over safety under fire conditions.

1.2 Moss Spheres

During the period of 1969-1972 the Kvaerner group and the DNV classification society collaborated to bring the Moss sphere into existence. Consisting of four to six aluminum alloy spheres the typical configuration of a Moss sphere vessel has a capacity of $125\,000\,m^3$ though vessels with capacities as low as $20\,000\,m^3$ and as large as $150\,000\,m^3$ are in service. The spheres are supported by an equatorial skirt of steel which serves to mount them to the vessel. They consist of an outer steel weather shield, an air gap, and a layer of insulation with a thin $(0.3\,mm)$ foil covering on its exterior (Figure 1.1). The insulation layer is made of polymeric foam and in general polyurethane, polystyrene or phenol resins are used. [15]While these foams have excellent thermal resistivity they do have relatively low degradation temperatures. This paper focuses on polystyrene (PS) foam insulation.

1.3 Polystyrene Insulation

Polystyrene was one of the first polymers to be commercialized. The discovery of its monomer constituent was attributed to Newman who isolated it by the steam distillation of cinnamic acid
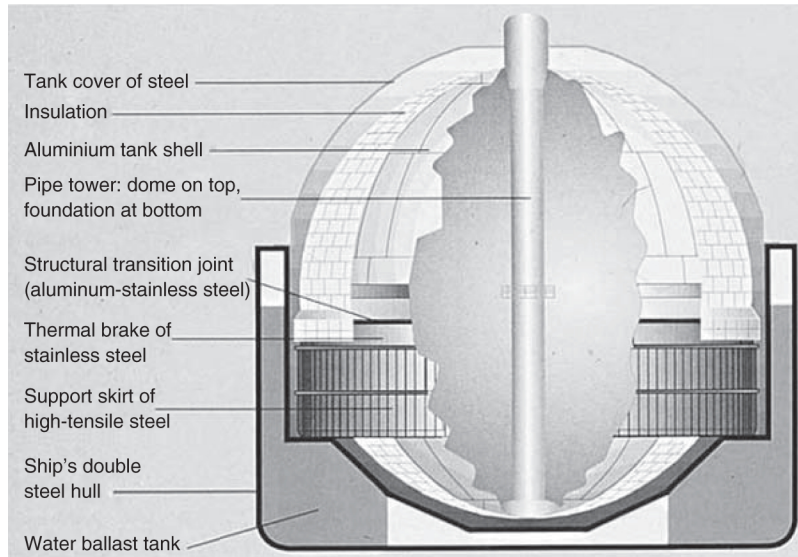
2

Figure 1.1: Cross Section of a Moss Sphere (Gaztransport & Technigaz)
[15]

obtained from amber. [8] The first successful polymerization occurred in 1839 by E. Simon who believed that he had created an oxidation product and so called it styrol oxidel [4]. Polystyrene is a solid below about 100 °C where it reaches its glass transition point. Because it is non-polar, chemically inert and non-reactive with water it has found many uses from coffee cups and commercial insulation to lost foam casting.

Current production of the styrene monomer comes from the dehydrogenation of ethyl benzene over a ferric oxide catalyst. From here there are many paths to the polymerization of styrene and depending on which one is used the specific characteristics of the polymer may be manipulated. [8]

There are two categories of foamed PS: expanded polystyrene (EPS) and extruded polystyrene (XPS). XPS is formed by placing granules of PS into an extruder where critical additives are combined with PS. The PS is then injected with a blowing agent after which the molding process creates the finished XPS product. Examples of this process include the blue and pink insulation products commonly used in housing. In the creation of EPS, PS is polymerized in suspension along with the blowing agents. A second process is then used to expand the beads into a mold [6].

This creates the glued bead look that is often seen in items such as packaging and coffee cups.

1.4 Society of International Gas Tanker and Terminal Operators Ltd. (SIGTTO) Work Group

In 2004 SIGTTO was approached with concerns about the sizing of the pressure relief valves(PRV) on LNG shipping vessels insulated with non fire-resistant materials. In the current method for sizing PRV it was unclear to what extent if at all the conditions resulting from a loss of insulation were taken into account. As the polystyrene used in the moss sphere type containers would be exposed to possibly damaging heat fluxes in the event of a fire on deck or near the ship concerns were raised pertaining to its effectiveness under extreme circumstances. In response, SIGTTO organized a working group consisting of various industry partners and universities to analyze possible oversights in the regulations. The working group was specifically tasked with determining the response of LNG vessels under the event of an enveloping pool fire that could be caused by the spillage of LNG. While most of the topics investigated by this report reached a consensus, concerns remained about the response of polymeric foams to fire conditions. Out of this working group two recommendations were made:

1. "If large scale LNG fire tests are carried out by Sandia, or others, that show significant conflict with existing values of heat flux used in the IGC Code and other industry codes and standards, the question of the current equations for determining fire-case pressure relief loads merit re-examination by the whole LNG industry and not just the shipping element."

2. "Although the working group has determined that current polystyrene foam insulated Moss sphere LNG carriers are equipped with pressure relief valves that provide additional capacity to prevent failure by over-pressure of intact cargo tanks, a better understanding of the foam plastic insulation vulnerability to heating is required to adequately assess the hazards that could result from loss of insulation effectiveness with fire exposure. Given the comparatively short duration of LNG fires as estimated by previous fire scenario studies, a much

4

better understanding of the temporal response of foam plastic insulation materials is necessary to determine the worst case circumstances as referred to in the conclusions above. Further research, which should include physical insulation testing as well as a determination of the potential for additional damage due to combustion of the foam degradation products, is recommended." [12]

This thesis addresses the second recommendation by providing new experimental measurements on the decomposition rates of polystyrene foam as a function of applied heat flux.

Chapter 2

Background

2.1 Current Modeling of LNG Container Performance

To understand decomposition of polymeric foams in LNG containment system we must look closely at the conditions which they would be exposed to in the event of a large scale fire. There are many possible fire scenarios that could lead to these conditions and each has its own parameters for modeling, but the most significant factor as far as the rate of PS degradation/decomposition is concerned is the heat flux that reaches the surface of the foam insulation layer. Current IGC code assumes an emissive heat flux from the fire of $108\,\text{kW/m}^2$ to determine pressure valve sizing. While this is a good place to start the body of research surround LNG pool fire emissivity indicates that the flux from a LNG pool fire may reach up to $350\,\text{kW/m}^2$ depending on the conditions and measurement procedure. To this end the SIGTTO working group modeled the response of the LNG containment system for conditions ranging from the IGC standard to $300\,\text{kW/m}^2$ and reported on the times to failure. [12]

Using these bounds to guide the modeling Kabelac et. al constructed a 1-d steady state analysis of the Moss sphere (figure 2.1). They determine that the maximum emissive flux of a $300\,\text{kW/m}^2$ fire to the interior was around $150\,\text{kW/m}^2$ (figure 2.2). Their analysis of this system also looked at the effects of the surface emissivity. Calculation performed during this investigation show that from a stand point of flux received by the foam layer there are two critical factors in the determining the emissive flux received: the temperature of the steel weather cover and the emissivity of the foam surface (aluminum foil shield). [12]

A simple calculation using the Stephan-Boltzmann law can be used to determine the relative emissive power of the weather cover to the foam as a function of their temperatures:
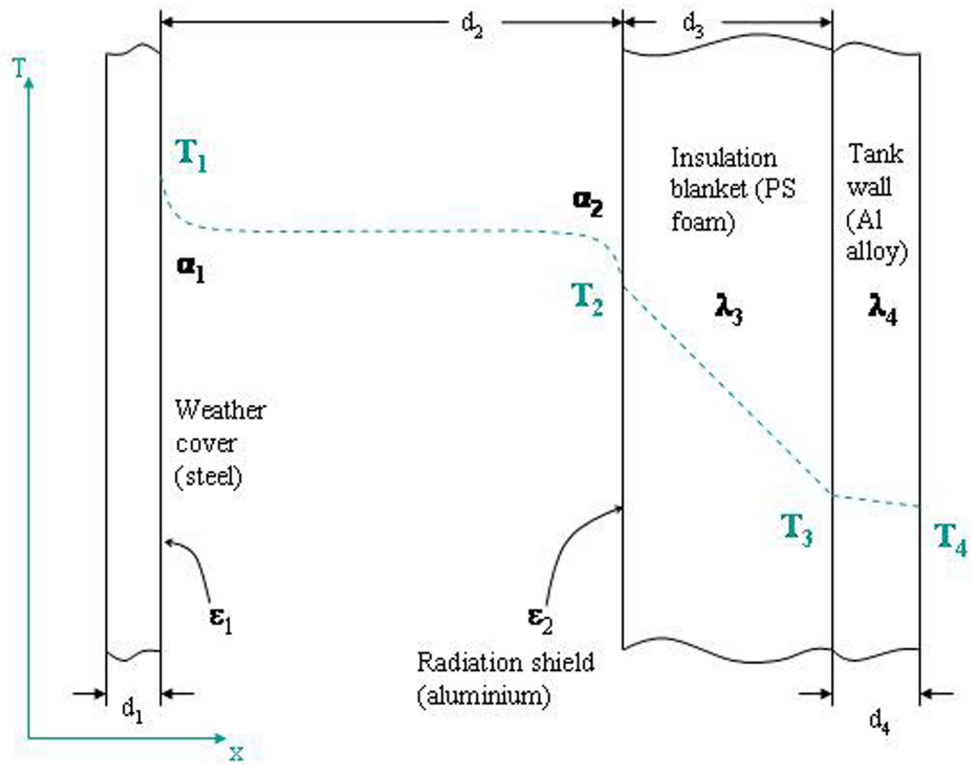
$$j = \varepsilon\sigma T^4 \tag{2.1}$$

6

Figure 2.1: One Dimensional Model of LNG Tank [12]
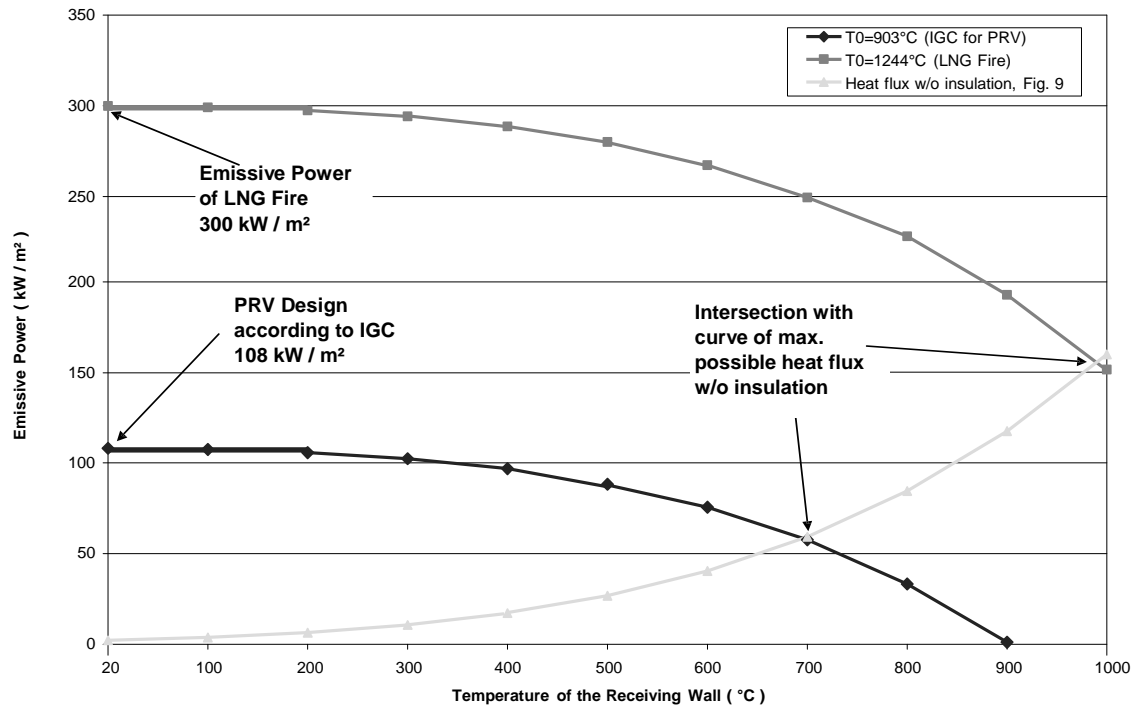
Figure 2.2: Maximum Emissive Power [12]

where:

- j = emissive power, kW/m^2

- σ = Stephan-Boltzmann constant, $5.67 \times 10^{-8} \, J/(s \, m^2 \, K^4)$

- T = surface temperature, W/cm^2

- ε = emissivity

Using BCM's value for the vaporizing surface of $447\,^\circ C$ and the upper bound outlined by Kabelac et al. we can get a clear range of about $1\text{-}10 \, kW/m^2$ absorbed into the surface with the aluminum radiation shield fully intact and its emissivity indicative of a clean surface, 0.07 (Figure 2.3). It can be seen clearly here how much the condition and efficacy of the thin aluminum heat shield plays in retarding the heating rate of the polystyrene insulation.

8

Figure 2.3: Emissive Power of Weather Cover to Polystyrene Insulation at 447 °C

2.2   Polystyrene Foam Thermal Response

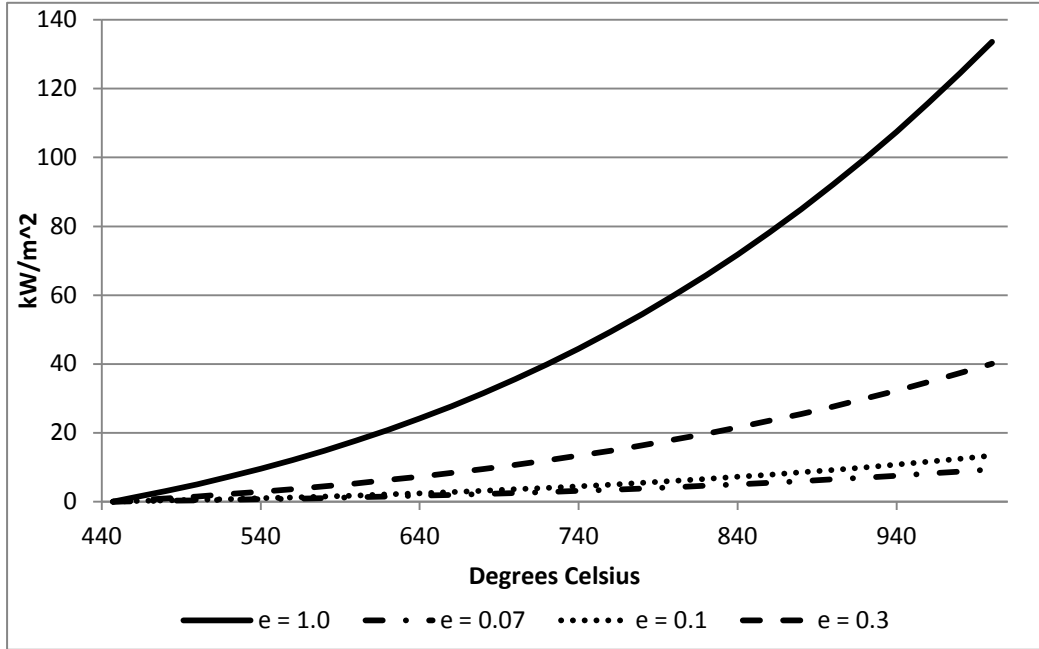Much of the research into polystyrene foam thermal response has been directed towards the analysis of expendable pattern casting (EPC) processes also known as lost foam casting (LFC). In this process, a desired shape is molded out of extruded polystyrene foam (XPS) and then packed into sand. Liquid metal is then fed under pressure into an opening in the mold and allowed to displace the foam. As the liquid metal front advances depending on the local conditions in the mold, the foam may be decomposed by more than one mechanism. In the models proposed by Barone and Caulk for the ablation and melting pathways the polymer leaves the system after undergoing some partial decomposition into a liquid and vapor phase [2] [5]. Because of this it is difficult to draw direct correlation about the temporal response of the foam to the rather more passive radiant heating conditions experienced under a weather shield.

A detailed study of the stages of degradation undergone by PS foam beads is quite informative for a qualitative understanding of the foam degradation process. The stages of thermal decom-
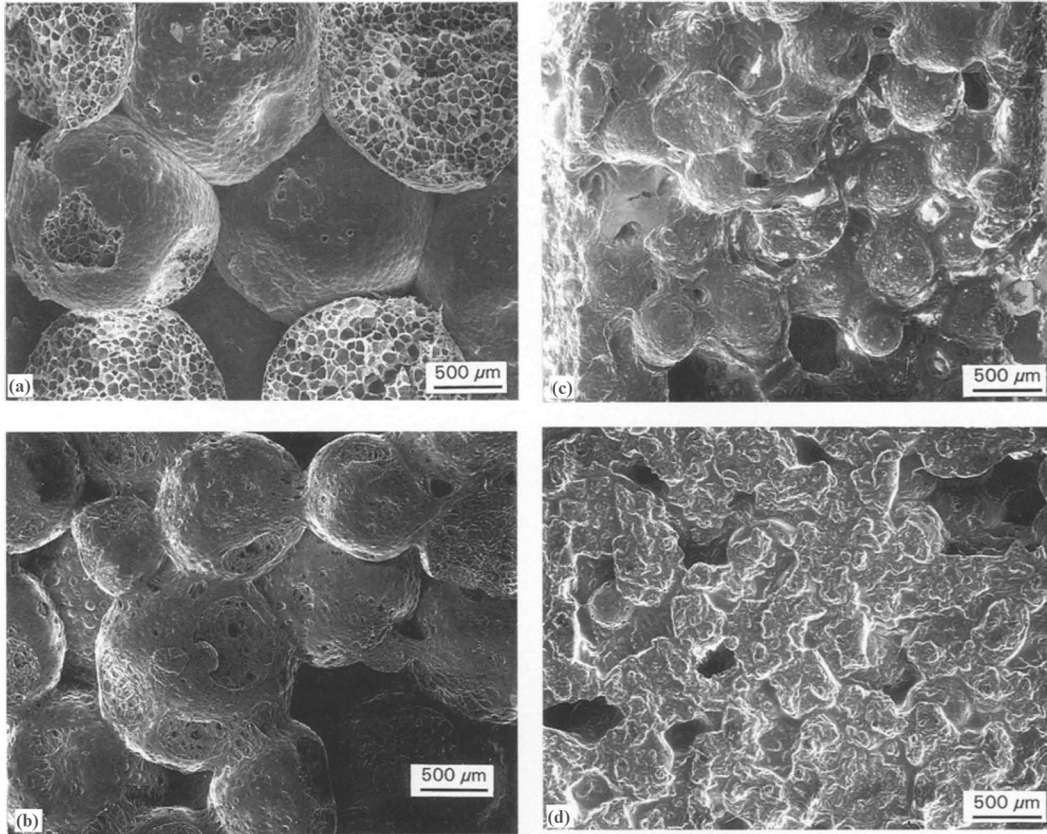
Figure 2.4: Photograph showing effects of temperature on bead structure(EPS initial density = $0.024 \, \text{g/cm}^3$) (a) $80 \, ^\circ\text{C}$, (b) $110 \, ^\circ\text{C}$, (c) $120 \, ^\circ\text{C}$, (d) $160 \, ^\circ\text{C}$ [9]

position of expanded polystyrene beads (EPS) has three major ranges:bead collapse, melting, and vaporization. By dipping $1.5 \, \text{cm}^3$ samples of EPS into water(for temperatures up to $100 \, ^\circ\text{C}$) and wax (temperatures up to $170 \, ^\circ\text{C}$) for 30 s, the effects of temperature on bead formation and over-all polymer condition were observed (Figure 2.4). At $160 \, ^\circ\text{C}$ it can be seen that the beads have completely melted forming a viscous residue. [9]

As the temperature increases past $170 \, ^\circ\text{C}$ the viscosity decreases until the vaporization point is reached. The DSC and TGA analysis from Mehta et al. indicated that vaporization begins around $275 \, ^\circ\text{C}$ and most all of the sample is vaporized by $460 \, ^\circ\text{C}$. A value of $912 \, \text{J/g}$ was also determined for the latent heat of vaporization. [9]

10

2.3   Polystyrene Degradation during Combustion

For a more quantitative look into the thermal degradation of PS we look to Brauman, Chen and Matzinger (BCM) and their approach to determining its combustion characteristics and corresponding pyrolization rates.

BCM created a "novel rod driven apparatus" to measure the combustion rates of polystyrene. A quartz sleeve mounted vertically in a 15 cm diameter chimney was used to house 6 and 10 cm lengths of 1.2 cm diameter Dow Styron 666U PS rods. Carbon black was added at 0.05% by weight to prevent incident radiation from being absorbed in the polymer bulk. The rods were ignited from the top and as the surface burned away the rods were advanced by a syringe pump. The drive rate of the syringe pump was adjusted to match the burning consumption rate so that the surface of the molten polystyrene stayed level with the top of the quartz sleeve. This velocity of advance divided by the surface area gave the mass loss rate per surface area during combustion. [3]

The same procedure was then carried out using infrared lamps as the heat source instead of combustion. A water cooled shield was added around the quartz sleeve to prevent the sample from heating at the sides. (Figure 2.5) The samples were replaced by a radiometer to independently measure the flux emitted by the spot heaters. A heating rate of $56.5 \, \text{kW/m}^2$ was found to match the regression rate during combustion. This corresponded to an absorbed flux of $14.9 \, \text{kW/m}^2$. [3]

2.3.1   Mass Loss Rate under Pyrolysis Conditions

To calculate the heat required to generate a unit mass of vapors Brauman et al used a technique developed by Tewarson to calculate the heat absorbed by the pyrolization process and the heat loss to the surroundings. Using a steady state energy balance over the sample rods yields the following analysis:

$$\dot{m} = (\dot{q}_{ext} - \dot{q}_l)/H_{rvum} \tag{2.2}$$

where:

- $\dot{m}$ = mass flux, $\text{g/(cm}^2\,\text{s)}$
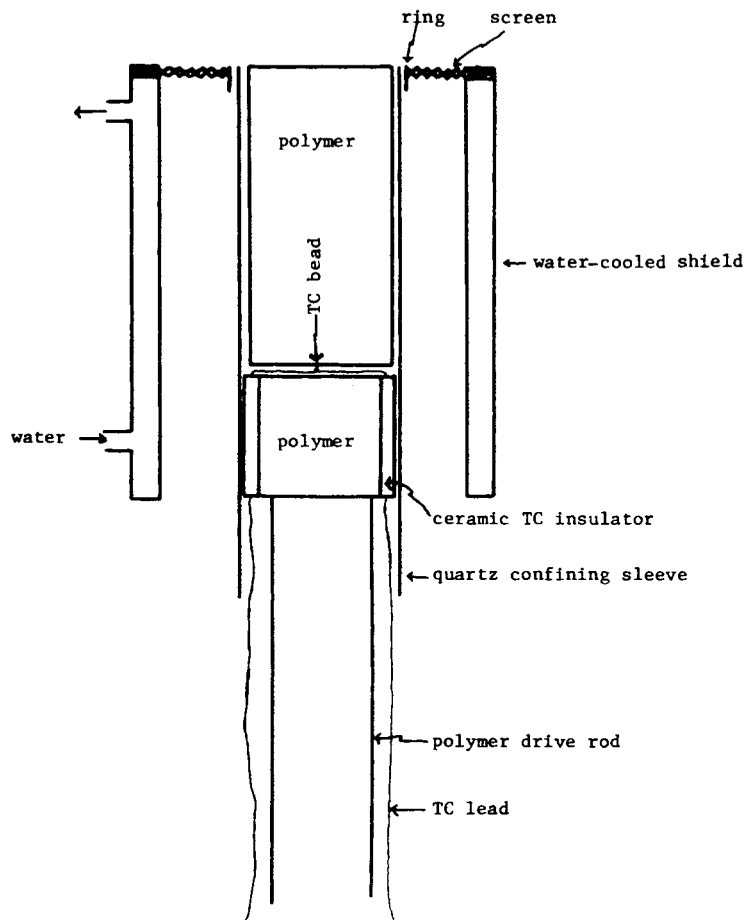
11

Figure 2.5: Schematic Diagram of Polymer Rod with Light Shield [3]

- $\dot{q}_{ext}$ = incident heat flux, W/cm^2

- $\dot{q}_l$ = heat loss to the surroundings, W/cm^2

- H_{rvum} = heat required to vaporize a unit mass, J/g

When $\dot{q}_l$ is constant, a plot of $\dot{m}$ verse $\dot{q}_{ext}$ yields a straight line with an intercept of $\dot{q}_l/H_{rvum}$ and a slope of $1/H_{rvum}$. [14]

Using this method BCM calculated the total heat required to vaporize a unit mass of PS to be $1980\,J/g$ and the heat loss to the surrounding for their apparatus to be $41.6\,kW/m^2$. While they did not report on foamed PS samples it seems reasonable that the technique used should be applicable to PS foams and provide insight into the degradation rate for these polymer products as well.

Chapter 3

Procedure and Results

The thesis of this work is an application of the technique Brauman, Chen, and Matzinger (BCM) used in their study of polystyrene (PS) combustion applied to the pyrolysis of extruded polystyrene (XPS) under similar heat fluxes. Three modifications to the apparatus used by BCM were made. Dow Styron 666d was used in place of 666u as 666u was not attainable. Since radiant pyrolysis was the only method of thermal degradation, i.e., no combustion, instead of having a separate cooling jacket and chimney the dimensions of our apparatus were modeled after the cooling jacket itself. As this reduced the overall size of the void space in the apparatus, the purge nitrogen was reduced accordingly to maintain laminar flow. The linear degradation rate of PS and XPS samples as a function of heat flux were recorded. From these data, the heat required to vaporize a unit mass was determined and compared with the results of BCM as well as to differential scanning calorimetry (DSC) and thermo gravimetric analysis (TGA) of the XPS and PS samples.

3.1 Experimental

3.1.1 Polymer Samples

For the solid polystyrene (PS), samples of Dow Styron 666d PS were ordered from the Spiratex Company (Romulus, MI) mixed with 0.05 percent by weight carbon black and extruded into 2 m long by 1.2 cm diameter rods. Due to variations in the diameter of the rods as received, they were milled to 1.08 cm diameter and then cut to a 10 cm length. The extruded polystyrene (XPS) samples were taken from Dow Styrofoam 1 in thick foam board panels. A hot wire apparatus was used to cut down the samples from their original size to 1.12 cm diameter by 15 cm length. The larger diameter and length of the XPS sample was necessary to accommodate the higher rates of regression of the less dense foam structure.

3.1.2 Apparatus

The polymer samples were mounted vertically inside a 1.2 cm, 15 cm long quartz sleeve centered in a 2.2 cm i.d., 15 cm long steel cooling jacket purged with nitrogen. The quartz sleeve served to contain the molten sample from running off as well as maintaining a constant surface area for heating. As the samples were heated from the top, the surface was pyrolyzed. The regressing top layer was maintained at a constant level with the top of the quartz sleeve by an advancing syringe pump (model 355, Sage Instruments, White Plains, NY). The advancement rate of the drive rod and assembly was adjusted so that it compensated for the regression rate of the polymer.

The radiant heat source was provided by two halogen lamp spot heaters (model 4085, Research, Inc., Minneapolis, MN) mounted opposite each other 40° from vertical and focused on the sample. The flux was regulated by a powerstat (Model 5420 SCR, Research, Inc., Minneapolis, MN). Direct calibration of the heating device control was not possible due to the coarseness of the controls. For this reason, before each run, the flux was measured and set by substituting a calorimeter (Gardon gauge, Medtherm Model 64-15-20) in place of the sample and its housing. A lockable swing arm was used so that the pyrometer window and the sample could be easily switched while ensuring that the gauge and the sample were placed at the same position in the radiant heat field.

The cooling jacket served both as a holder for the quartz sleeve and sample as well as a shield for the shaft of the rod from the heat lamps. To further ensure that the sample received no radiation along its length a stainless steel disc with mesh vents was placed around the top of the apparatus so that the gap between the quartz sleeve and the cooling jacket was shaded. This disc, held in place by a metal collar, also provided stability for the quartz sleeve and maintained its position in the center of the apparatus. Water flowing through the shield maintained the interior of the jacket at ambient temperature.

To provide another point of comparison with the data collected by BCM a thermocouple was used to measure the temperature profile of the solid polystyrene as a function of depth. A hole was drilled to the center of the sample and a trough was milled from the hole to the bottom of the sample to permit the thermocouple wires to pass without binding the advancement of the sample
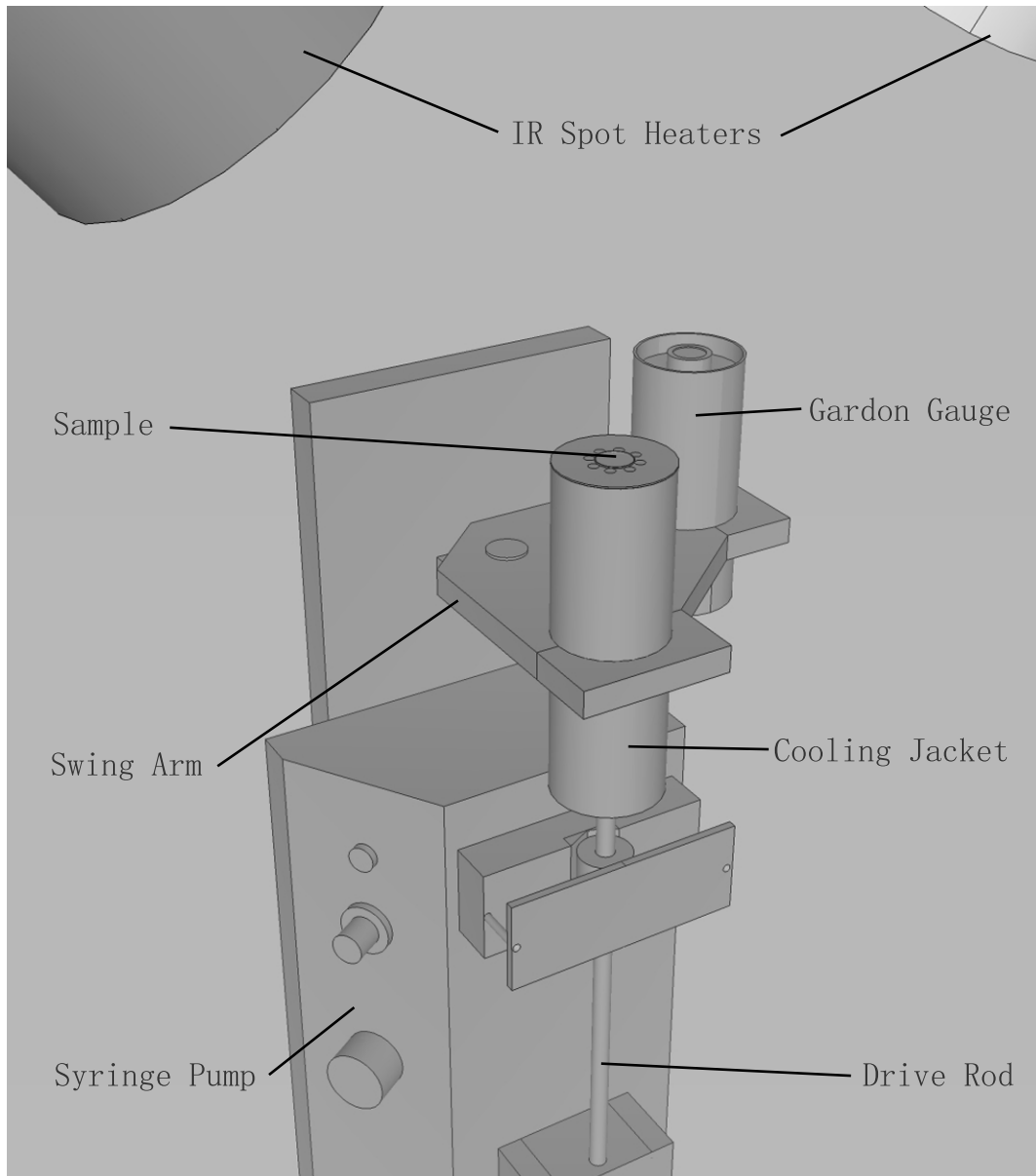
Figure 3.1: Apparatus Diagram

in the quartz sleeve. Attempts to perform the same test on the XPS rods were not successful due to the velocity disparity between the melt zone and the bulk of the rods due to the density change across the melting boundary.

3.1.3 Procedure

Before each run the vent hood was turned on, the water rate to the cooling jacket and the pyrometer were stabilized and recorded, the air cooling rate to the lamps was set and recorded, and the nitrogen purge rate set. The pyrometer was locked into position below the focal point of the heat lamps and then the rheostat adjusted to dial in a certain mV output which could then be converted using a calibration curve provided by a recalibration done by Medtherm. After the voltage reading from the radiometer was stable the lamps were shut off and the sample was rotated into position below the focal point of the lamps. The lamps were then turned on and the rate of the syringe pump was adjusted to maintain a level surface.

The drive rates for the syringe pump were manually recorded vs time and then converted to polymer regression rates using a calibration curve created from a plot of drive rate in cm/min vs the dial reading. In the solid polymer sample case, the experiments were run until the drive rate was stable for ten minutes. The value of the drive rate during this period was used to represent the steady state degradation rate at the chosen heat flux. For the foamed polymer samples, the same process of recording drive rate vs. time was used but the length of the run was limited by the amount of polymer available for vaporization. Because of this the XPS samples were run to the same state of completion of pyrolysis by stopping the runs when 2 cm of the samples remained. The average over the final 2 minutes of each run was used. The much shorter time period on the XPS was due to the rapid rate of regression on the samples, the shortest of which finished in just under 3 minutes.

The mass loss rate was measured and plotted as a function of the incident flux rate. PS samples were run from $49.6\,\mathrm{kW/m^2}$ to $62.8\,\mathrm{kW/m^2}$ and XPS samples from $27.4\,\mathrm{kW/m^2}$ to $45.1\,\mathrm{kW/m^2}$. These linear rates were then converted into mass loss rates using the density of the sample and the

volume consumed. For the PS rods, this density was $1045\,\mathrm{kg/m^3}$ and for the XPS rods the density was $25.6\,\mathrm{kg/m^3}$. A linear regression of the mass loss rate plotted against the incident flux was used to calculate the total heat of gasification, H_{rvum}, and the heat loss due to re-radiation and convection to the apparatus, $\dot{q}_l$. The results for the total heat of gasification were compared to TGA and DSC data provided by Netzsch Thermo-graphic^{TM}.

3.1.4 Sample Calculation

From the run on sample 27 (Figure 3.2) of the PS foam we first calculate the time weighted average of the syringe pump rate over the last 120 seconds of the run (Table 3.1).

$$R_{avg} = (\sum_{i=t_f-120}^{t_f} (t_{i+1} - t_i)R_i)/120 \tag{3.1}$$

where:

- R_{avg} =Average Pump Reading

- R_i =Pump Reading at a Given Time

- t_f =Time of Final Measurement, s

- t_i =Time of Measurement, s

- t_{i+1} = Time of Next Measurement, s

The value for R_{avg} is then compared to the calibration curve for the syringe pump and the linear rate of the sample advancement is recorded.

$$v_r = R_{avg} * m_p \tag{3.2}$$
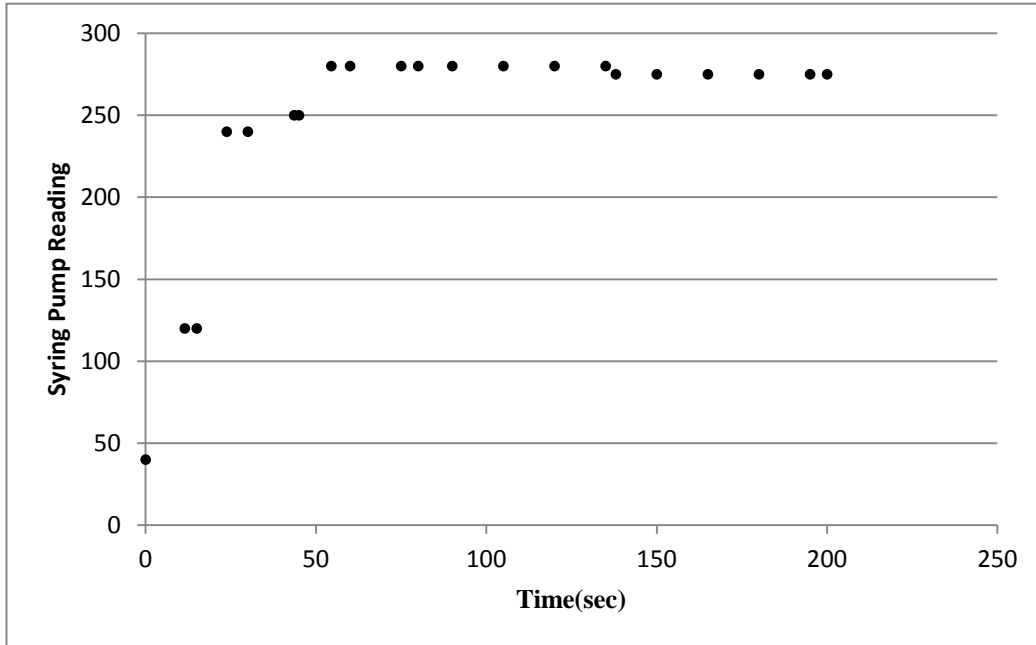
where:

- R_{avg} =Average Pump Reading

18

Figure 3.2: Run 27, mV=1.84

Table 3.1: Run 27 - Last 120 Seconds.

DialReading	Time (sec)
80	280
90	280
105	280
120	280
135	280
138	275
150	275
165	275
180	275
195	275
200	275

- v_r =Ram Velocity, cm/s

- m_p =Slope of Pump Calibration Curve, 0.01401 cm/s

This value is then converted into the mass loss rate by using the density and ratio of the cross sectional areas of the sample and the quartz sleeve.

$$\dot{m} = v_r * A_s / A_q * \rho \tag{3.3}$$

where:

- $\dot{m}$ =Mass Consumption Rate Per Unit Area, $g/(s\,cm^2)$

- v_r =Ram Velocity, cm/s

- A_s =Cross Section Area of Sample, cm^2

- A_q =Cross Section Area of Quartz Sleeve, cm^2

- ρ =Density of Sample, g/cm^3

The value for the incident radiant heat flux is calculated similarly from the slope of the calibration curve for the radiometer.

$$q_{ext} = V_r * m_r \tag{3.4}$$

where:

- q_{ext} =Incident Heat Flux

- V_r =Radiometer Voltage Reading, mV

- m_r =Slope of Radiometer Calibration Curve, 22.13 $kW/(m^2\,mV)$

Using equations 3.1-3.4 a value of $13.39 \times 10^{-4}\,g\,s^{-1}\,cm^{-2}$ was found as the regression rate of the foam at an external flux of $40.72\,kW\,m^{-2}$ for run 27. The results from each of the runs were tabulated in this fashion and graphed to provide data on H_{rvum} and q_l.

3.2 Results

3.2.1 Repeat of Bruamen et. al.

The mass loss rates as a function of external heat flux received are shown in figure 3.3. The BHW values are from our apparatus and the BCM values are reproduced from the data provided in BCM in 1983. Using equation 3.1 t he values of H_{rvum} and $\dot{q}_l$ indicated from figure 3.3 are:

- BCM: $H_{rvum} = 1980\,\mathrm{J/g}$; $q_E = 41.6\,\mathrm{kW/m}$

- BHW: $H_{rvum} = 1592\,\mathrm{J/g}$; $q_E = 42.8\,\mathrm{kW/m}$

The values of H_{rvum} for the solid PS rods were 20% lower than the values reported by BCM. The difference may have been due to the substitution of the Styron 666d in place of the Styron 666u or it may have been due to the calibration curve used for the spot heaters. The wide variance in the values reported for each flux seems consistent with the coarseness of the spot heater power stat used in the repeat experiment and would throw a large error into any experiment based on its dial readings. Since the exact model of the power stat used in their experiment is not know and details of the procedure for determining the incident heat flux were not described, the consistency of its output at a reading cannot be determined.

The temperature profile of one of the PS samples is reported in figure 3.4. The temperature values were very close to that reported by BCM. A final temperature of 718.3 Kelvin was recorded as the thermocouple began to breach the surface of the liquid/vapor interface. This is consistent with the known properties of PS as well as the data reported by BCM in 83'.

3.2.2 Extruded Polystyrene Foam

Sample rods of XPS run with $27.4\,\mathrm{kW/m^2}$ to $45.1\,\mathrm{kW/m^2}$ fluxes gave mass loss rates as shown in Figure 3.5 along with the values for the PS samples for comparison. The XPS and PS degradation rates are quite similar when taken from the standpoint of mass loss rate. If we look at the linear degradation rate (figure 3.7) we can clearly see that since the total heat required to vaporize the
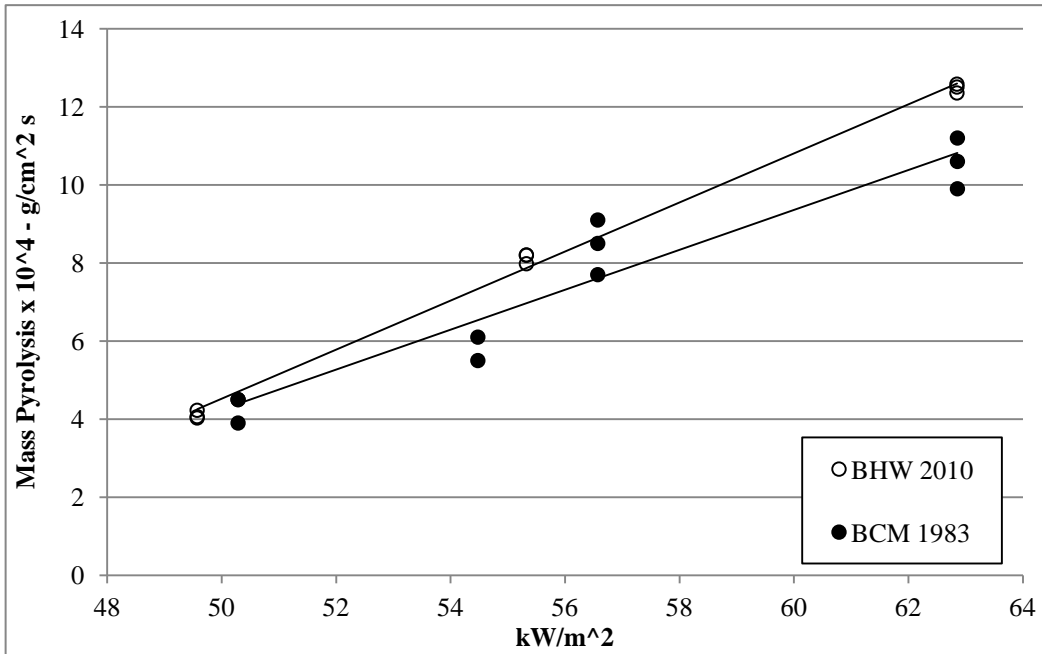
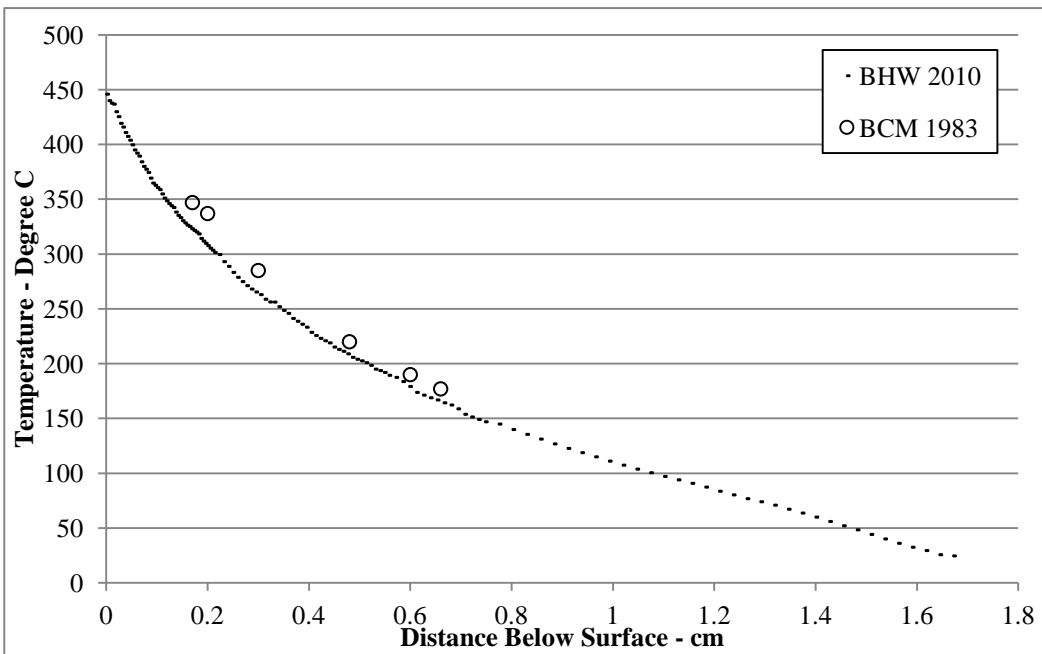Figure 3.3: Comparison with BCM: Mass Pyrolysis Rate of Solid Polystyrene as a Function of External Heat Flux

Figure 3.4: Center Temperature of PS Samples as a Function of Distance from the Surface
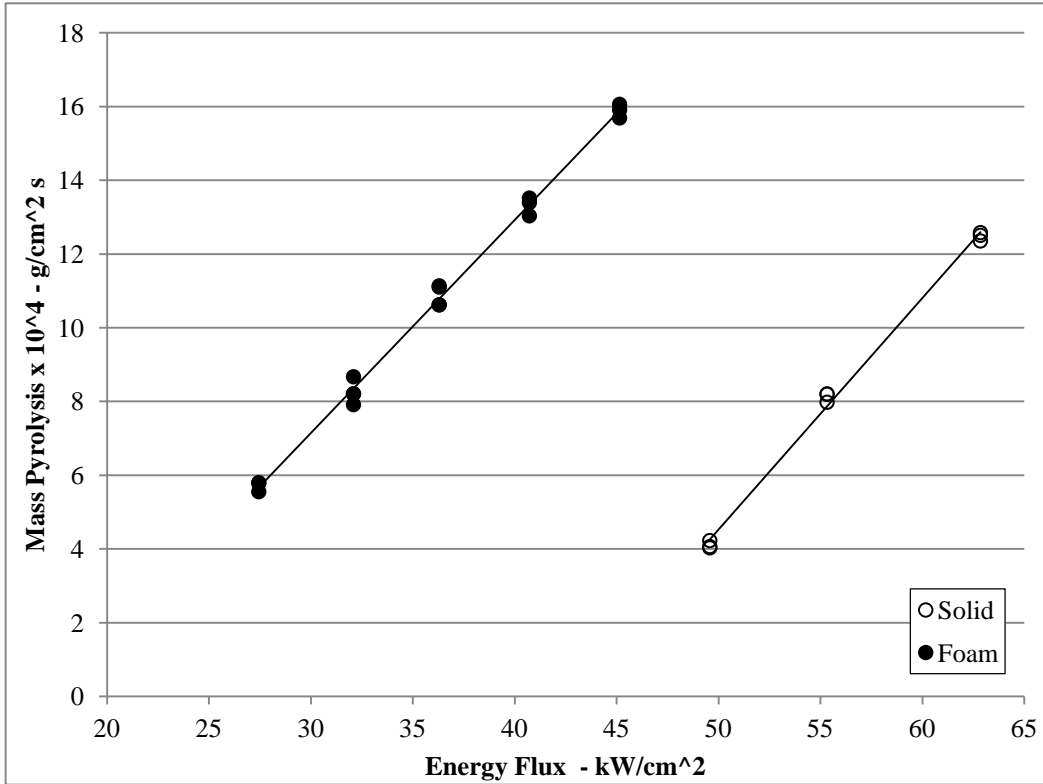
22

Figure 3.5: Mass Loss Rate of PS and XPS as a Function of External Heat Flux

samples is so close the difference in regression rate is almost directly proportional to the ratio of the densities or about 40 to 1. From figure 3.5 we can once again calculate the heat of gasification from the slope of the line and the heat loss to the surrounding from its intercept yielding:

- PS: $H_{rvum} = 1592\,\text{J/g}$; $q_E = 42.8\,\text{kW/m}$

- XPS: $H_{rvum} = 1693\,\text{J/g}$; $q_E = 17.6\,\text{kW/m}$

The most significant difference between these two values is the value reported for $\dot{q}_l$. This is most likely due to the difference in the thickness of the melt zone. In the PS samples the melt zone was between 8 mm and 9 mm and for the XPS it was around 2mm. The difference in these two zones is mostly due to the imperfect contact caused by the truncation of the foam as it entered the melt zone and the lower conductivity of the XPS. These two factors effectively provided insulation of the unmelted bulk slowing the heat penetration further into the sample. Since the PS samples did
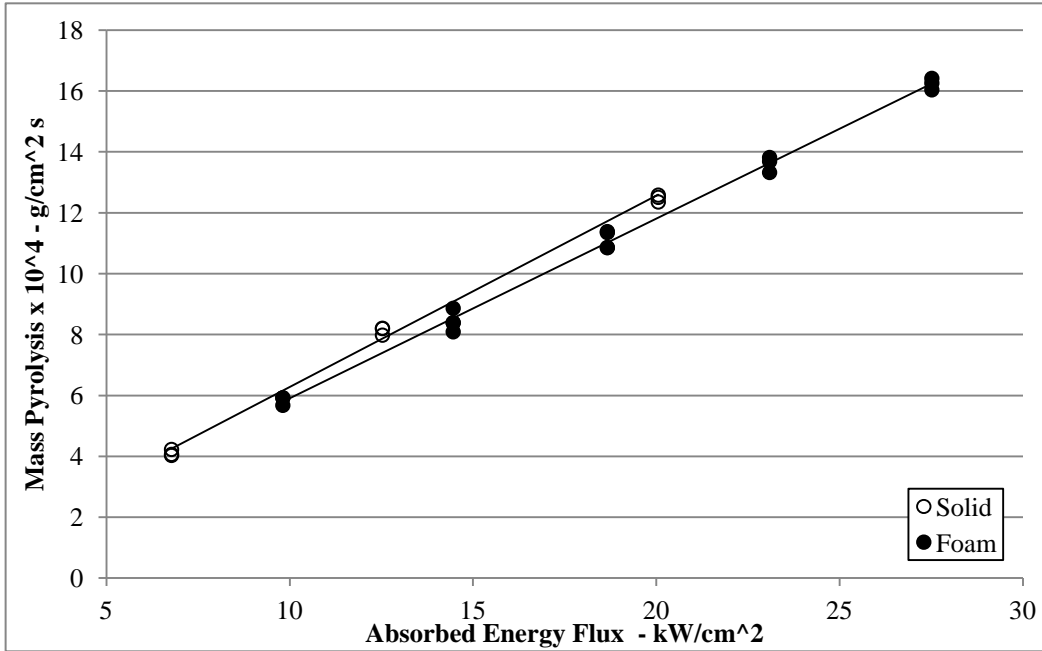
Figure 3.6: Mass Pyrolysis Rate as a Function of Absorbed Heat Flux

not have these obstacles the melt depth and therfore radiant heatloss was greater.

The similarity in the comparison of the XPS and the PS sample runs is more clearly shown when we subtract the heat loss, $\dot{q}_l$, from the incident flux, shown in figure 3.6. The linear decomposition rate as a function of absorbed heat is shown in figure 3.7.

3.2.3 DSC and TGA Analysis

Differential scanning calorimetry (DSC) and thermo gravimetric analysis (TGA) of samples of the PS and XPS were analyzed by Netzsch. Netzsch' analyses determined the heat capacity, C_p, and the heat of vaporization, H_{vap} [1]. From the C_p data provided by Netzsch (Figure 3.8), the C_p of both the PS and XPS was determined as a function of temperature.

From the linear regression of this C_p data the heat capacities of the XPS and PS as a function of temperature were determined to be:

- XPS: $C_p = 4.22T - 18; \mathrm{J\,K/g}$

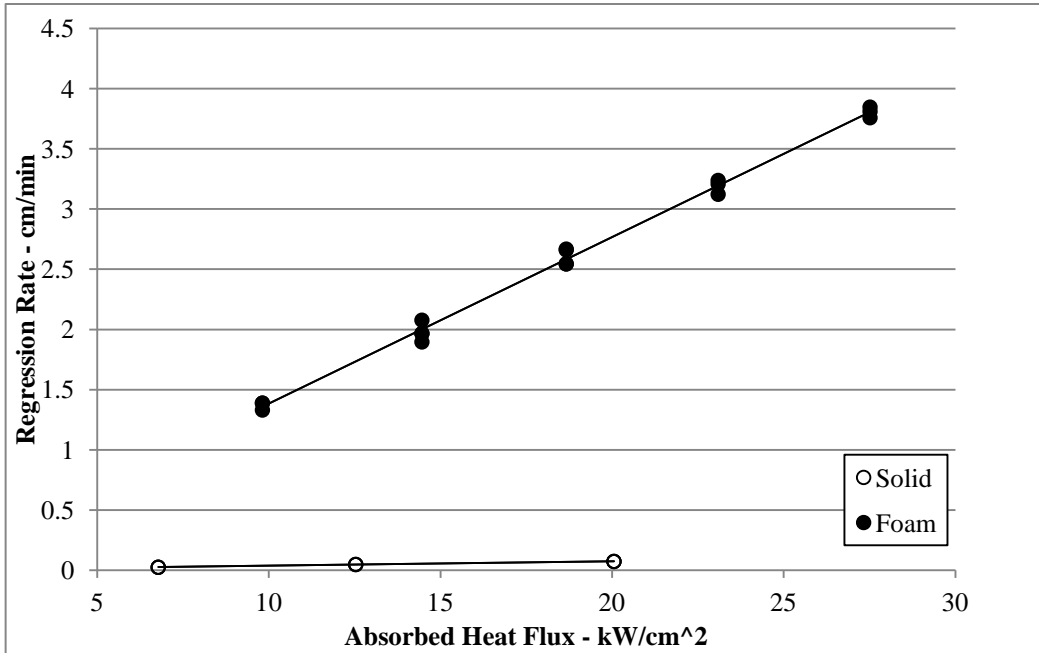- PS: $C_p = 4.50T - 180; \mathrm{J\,K/g}$

24

Figure 3.7: Linear Decomposition Rate of XPS as a Function of Absorbed Heat Flux

An independent analysis of the DSC data provided by Netzsch indicated that the vaporization began at 583 K and ended at 720 K [1]. The values for H_{vap} calculated by Netzsch were:

- PS:$H_{vap} = 592 \, \text{J/g}$

- XPS: $H_{vap} = 793 \, \text{J/g}$

Taking the C_p data and adding the H_{vap} a total heat of gasification from room temperature was calculated yielding:

- PS: $H_{rvum} = 1447 \, \text{J/g}$

- XPS: $H_{rvum} = 1580 \, \text{J/g}$

These values are within 10% of those calculated from our experimental results.
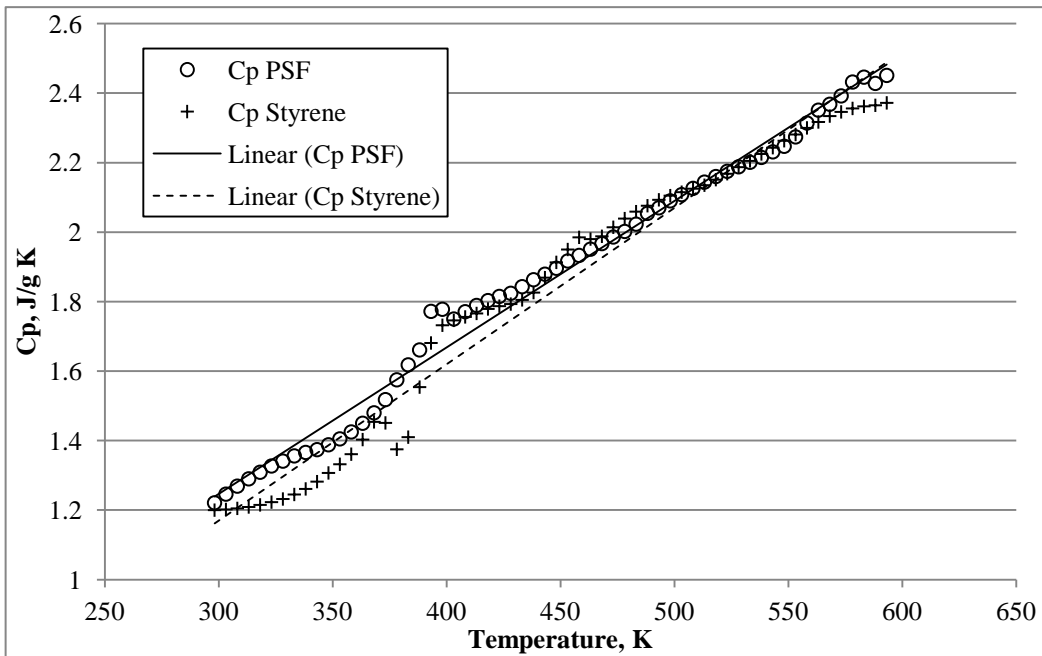
Figure 3.8: Specific Heat Capacities of PS and XPS
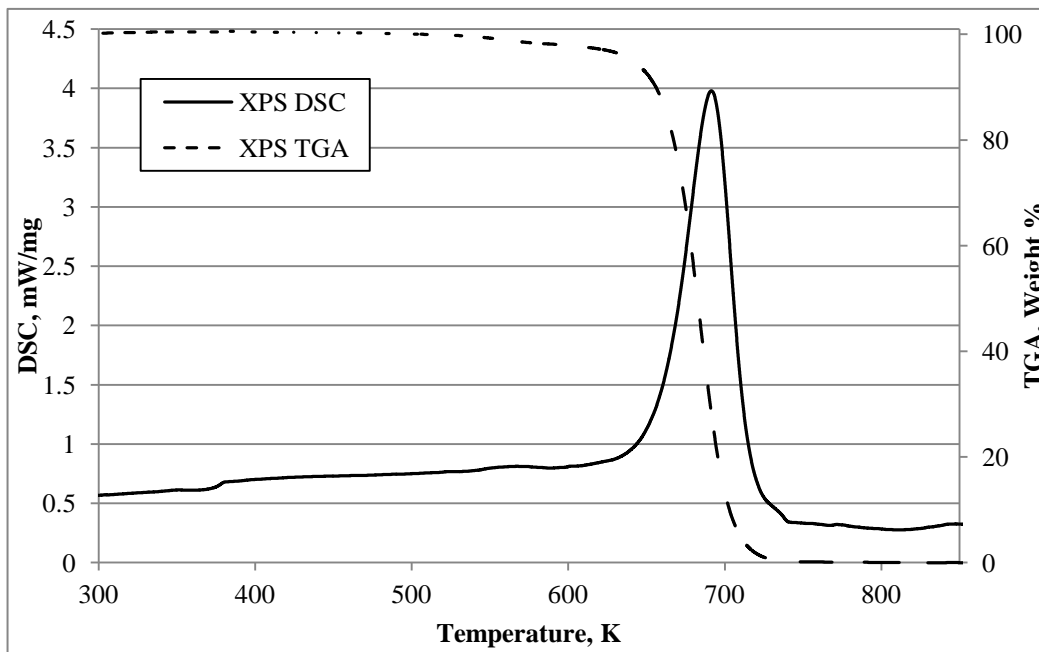

Figure 3.9: DSC and TGA Scans for XPS

26

Chapter 4

Conclusion

In this experiment absorbed heat fluxes into polystyrene were tested so that they were consistent with the range expected under the weather cover of an LNG carrier during a large pool fire. The ranges tested assumed that the insulation heat shield remained in place during decomposition. This is done partially to show a best case scenario, but largely because modeling the degradation of the aluminum foil shield is beyond the scope of this paper. Even with this protection, a significant rate of decomposition of the foam will occur under the conditions outlined by the SIGTTO working group consensus. The materials rate of decomposition appears to be primarily a function of its specific heat and its heat of vaporization. From these two variables the rate of mass loss can be determined as a function of applied heat flux and from the density we can then calculate the linear rate of decomposition. In the case extruded polystyrene insulation (XPS) a value of $1693\,\mathrm{J/g}$ was found to describe the energy necessary to decompose a unit mass from room temperature. For this material a foam a decomposition rate of around $1.38\,\mathrm{cm/min}$ is shown for a flux of $10\,\mathrm{kW/m^2}$.

The process of foaming PS to create XPS decreases both the density and the thermal conductivity of the material. These two changes account for the majority of the differences seen in the materials response to high heat fluxes. Lowering the density showed an inverse effect on the linear regression rates, causing the linear regression rates of the XPS to be higher than PS by almost the same ratio as their densities, or about 40 to 1. This suggests that the mechanics of the degradation in the XPS and the PS are very similar. As they are made of the same base material this is not surprising. The smaller depth of the melt layer when compared to the PS, while not having a direct effect on the final steady state regression rate, should lower the time required for a fully developed temperature profile to develop in XPS, leading to a shorter time period before the steady state decomposition rate is reached in the less dense material.

The DSC analysis of the PS and XPS samples show a some difference from the experimental

runs for the heat required to vaporize a unit mass (about 10%). This could be due to the different rates of heating that the material is undergoing. In the DSC a relatively low and constant rate of heating ($20\,^\circ$C/min) is occurring. This is a significantly different rate of heating than in the experimental setup for the XPS and PS sample runs. As there are a number of temperature dependent reactions that may happen as PS is being thermally decomposed the time spent at each temperature may affect the overall composition of the vaporization products and therefore the total energy absorbed by the material on its path to vaporization. DSC and TGA analysis of the overall heat absorbed at similar heating rates may provide a closer match to the observed total heat of degradation of PS materials at these conditions.

Further research into the reaction of the aluminum heat shield to these conditions is needed to provide an accurate description of failure times as used on LNG carriers. It seems likely that the aluminum shield will lose part or all of its effectiveness at some point during the foam decomposition which will greatly increase the rate of foam decomposition.

References

[1] Netzsch Instruments, Inc., 37 N. Avenue, Burlington, MA, 01803.

[2] M.R. Barone and D.A. Caulk. A foam ablation model for lost foam casting of aluminum. *International Journal of Heat and Mass Transfer*, 48(19-20):4132 – 4149, 2005.

[3] S. K. Brauman, I. J. Chen, and D. P. Matzinger. Polystyrene degradation during combustion. *Journal of Polymer Science: Polymer Chemistry Edition*, 21(6):1831–1845, 1983.

[4] J. A. Brydson. *Plastics Materials, 7th ed.* Butterworth-Heinemann, Wobum, MA, USA, 1999.

[5] D.A. Caulk. A foam melting model for lost foam casting of aluminum. *International Journal of Heat and Mass Transfer*, 49(13-14):2124 – 2136, 2006.

[6] Alexander B. Morgan Charles A. Wilkie. *Fire Retardancy of Polymeric Materials, 2nd ed.* CRC Press, Boca Raton, FL, USA, 2010.

[7] Dr. Chen-Hwa Chiu. History of the development of lng technology. AIChE Annual Conference, Chevron Energy Technology Company, November 2008.

[8] Graham Swift Hans R. Kricheldorf, Oskar Nuyken. *Handbook of Polymer Synthesis, 2nd ed.* Marcel Dekker, New York, NY, USA, 2005.

[9] S. Mehta, S. Biederman, and S. Shivkumar. Thermal degradation of foamed polystyrene. *Journal of Materials Science*, 30:2944–2949, 1995. 10.1007/BF00349667.

[10] Anay Luketa-Hanlin John Covan Sheldon Tieszen Gerry Wellman Mike Irwin Mike Kaneshige Brian Melof Charles Morrow Don Ragland Mike Hightower, Louis Gritzo. Guidance on risk analysis and safety implications of a large liquefied natural gas (lng) spill over water. Technical Report SAND2004-6258, Sandia National Laboratories, December 2004.

[11] Peter G. Noble. A short history of lng shipping. Texas Section SNAME, February 2009.

[12] Society of International Gas Tanker & Terminal Operators. *Report on the Effects of Fire on LNG Carrier Containment Systems*. Witherby Seamanship International Ltd, 2009.

[13] North American Mfg. Co. Richard James Reed. *North American Combustion Handbook: Combustion, fuels, stoichiometry, heat transfer, fluid flow*. North American Mfg. Co., 1986.

[14] A. Tewarson. Physico-chemical and combustion/pyrolysis properties of polymeric materials. Technical Report NBS-GCR-80-295, Factory Mutual Research, November 1980.

[15] John L. Woodward and Robin M. Pitblado. *LNG Risk Based Safety: Modeling and Consequence Analysis*. John Wiley & Sons Inc., Hoboken, New Jersey, USA, 2010.